Inorganic Chemistry

Article

pubs.acs.org/IC

Nanopatterning of Magnetic CrNi Prussian Blue Nanoparticles Using a Bacterial S-Layer as a Biotemplate

Elsa Valero,[†] Miguel Martín,[‡] Natividad Gálvez,[‡] Purificación Sánchez,[‡] Johannes Raff,[§] Mohamed L. Merroun,[∥,⊥] and Jose M. Dominguez-Vera*[,‡]

[†]School of Chemistry, The University of Edinburgh, David Brewster Road, Edinburgh, United Kingdom

[‡]Departamento de Química Inorgánica and Instituto de Biotecnología, Universidad de Granada, 18071 Granada, Spain

[§]Institute of Resource Ecology and Helmholtz Institute Freiberg for Resource Technology, Helmholtz-Zentrum Dresden-Rossendor, Bautzner Landstrasse 400-01328 Dresden, Germany

[∥]Institute of Resource Ecology, Helmholtz-Zentrum Dresden-Rossendor, Bautzner Landstrasse 400-01328 Dresden, Germany

ABSTRACT: We have developed a simple process to fabricate on a bioplatform patterns of nanoparticles of a molecule-based magnet. Nanoparticles of the ferromagnetic Prussian blue derivative $Cs_xNi[Cr(CN)_6]$ were orderly deposited onto S-layers of *Lysinibacillus sphaericus*, forming a dense carpet of nanoparticles following the square lattice (p_4) pattern of the biotemplate. These results are encouraging to extend this approach by focusing on molecule-based magnets patterned into domains with controlled shapes and positions on a biosurface.

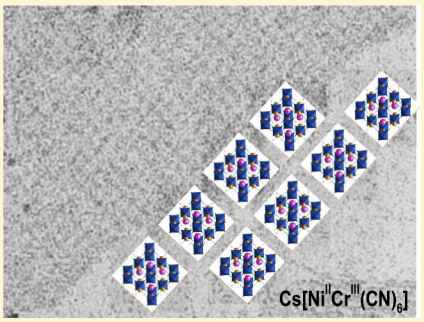

INTRODUCTION

The capability to deposit, in a controlled manner, magnetic nanoparticles on an adequate surface is a prerequisite to exploring the potential applications of magnetic devices relevant to the emerging field of molecular electronics. Presently, developments in colloidal synthesis permit a fine control of morphological characteristics of magnetic nanoparticles such as size and shape, but much effort is required for their ordered deposition, which would open the possibility to tailor new devices.

In this field, the most common magnetic nanoparticles checked consist of ferromagnetic zerovalent metal nanoparticles.[1,2] However, other kinds of magnetic nanoparticles, like those of molecule-based magnets, have also been deposited onto different substrates.[3−7] The family of Mn_{12} clusters and Prussian blue derivatives are two genuine examples. In particular, the interest in magnetic Prussian blue nanoparticles lies in the extraordinary variety of their additional physical properties (electrochromism, photomagnetism, piezomagnetism, etc.),[8−14] which opens prospects for making original functional nanomaterials. Likewise, an additional advantage of molecular magnets consists in their solubility in common solvents, which facilitates the positioning of nanoparticles onto selective portions of the substrate. Along these lines, several chemical and physical approaches for controlled deposition of these kinds of nanoparticles have been investigated, including microcontact printing,[7] photolithography,[12] self-assembly by water-droplet templates,[16] and local oxidation nanolithography.[17,18] Nevertheless, development of methodologies based on the ordered deposition of nanoparticles on solid substrates directly from solution is highly desirable.

In this sense, an alternative and elegant approach to the more conventional surface methodologies to integrate magnetic nanoparticles into patterned devices is based on the use of microorganisms as bioplatforms for arranging (in some cases producing and arranging) nanoparticles.[19−21] Here, we present an approach based on the bacterial cell surface layers (S-layers) that leads, using a simple and fast process, to patterning of nanoparticles of a Prussian blue derivative over large areas of the S-layer substrate. The pattern is fabricated by molding a water suspension of $Cs_xNi[Cr(CN)_6]$ nanoparticles on a structured S-layer matrix.

S-layers represent the outermost cell envelope component in a broad range of bacteria and archaea. They are monomolecular arrays composed of a single protein or glycoprotein. They are highly porous protein meshes with unit cell sizes in the range of 3 to 30 nm and pore sizes of 2 to 8 nm. S-layer proteins exhibit the capability to form free-floating self-assembly products in solution with different patterns (e.g., flat sheets, tubes, vesicles), which makes them very attractive to use as a template for the fabrication of different nanopatterning.[22]

The highly ordered crystalline S-layers of some bacteria have been used as templates for direct precipitation of metals from solution or by binding preformed metallic nanoparticles.[22−28] However, no extension of this procedure has been applied to molecule-based nanoparticles.

Received: March 11, 2015
Published: July 7, 2015

DOI: 10.1021/acs.inorgchem.5b00555
Inorg. Chem. 2015, 54, 6758−6762

In the present study, nanoparticles of the ferromagnetic Prussian blue derivative $Cs_xNi[Cr(CN)_6]$ were deposited on an S-layer protein of *Lysinibacillus sphaericus* JG-A12 (formerly *Bacillus sphaericus* JG-A12) and were characterized by transmission electron microscopy (TEM), IR absorption spectroscopy, and SQUID techniques. It has been previously reported that the S-layer of *L. sphaericus* JG-A12 binds selectively and reversibly metals from heavy-metal-contaminated uranium wastewaters.[29] Likewise, zerovalent metal nanoparticles (Pd, Au, etc.) with sizes in the range 1−5 nm have been deposited on this S-layer.[30] The use of the predefined nanoporous pattern of an S-layer precludes uncontrolled aggregation of the nanoparticles and keeps their structural and magnetic integrity. This preliminary result is encouraging and opens the possibility to pattern a large amount of coordination nanoparticles, especially molecular magnets.

Chemical agents are frequently used during the synthetic process to control the growth of the particles to preclude their aggregation and ensure their dispersion in different solvents.

Mallah et al. have recently shown that such stabilization can be achieved in some cases, as in the $Cs_xNi[Cr(CN)_6]$ network, without the use of coating agents, thus leading to negative monodisperse particles with an average size of 6 nm.[31,32]

The inner surface charge of S-layers can be negative or positive, depending on the equity or excess of exposed carboxylic acid or amino groups. Working at acid pH, the protonation of amino groups is favorable and allows the interaction with negatively charged nanoparticles. Although there is no definitive proof of the nature of the bond between S-layers and nanoparticles, in principle, this interaction may be purely electrostatic, hydrogen bonding, or both. In this sense, the negatively charged $Cs_xNi[Cr(CN)_6]$ nanoparticles could be deposited by electrostatic interaction with positive NH_3^+ terminal groups at the S-layer and/or by hydrogen bonds since the surface of the $Cs_xNi[Cr(CN)_6]$ particles has N atoms belonging to the peripheral $Cr(CN)_6^{3-}$ fragment. Therefore, the choice of $Cs_xNi[Cr(CN)_6]$ nanoparticles to be patterned onto an S-layer seemed appropriate.

The production of the S-layer CrNi nanoparticles was carried out in a single-step procedure, by incubation of an S-layer of *L. sphaericus* JG-A12 with a water suspension of nanoparticles of the ferromagnetic complex $Cs_xNi[Cr(CN)_6]$ with an average size of 6 nm for 24 h at room temperature. Dynamic light scattering (DLS) measurements confirmed that no aggregations of particles took place in these conditions, showing the existence of a single population size centered on ∼6 nm. The mixture was centrifuged and resuspended several times until the supernatant solution contained a negligible concentration of Ni and Cr (see Experimental Section). The resulting powder was then dried and isolated.

Infrared spectroscopy on the powder showed two asymmetric vibrations, one intense at 2172 cm^{-1} and a low-intensity shoulder at 2130 cm^{-1} (Figure 1) assigned to bridging and nonbridging cyanides located in the core and at the particles' surface, respectively.[31,34]

TEM images of the deposited CrNi nanoparticles onto the S-layer are shown in Figure 2. Metallic cores were generally well-defined, showing irregular spherical-like topologies with a heterogeneous size (average size of 6.0 nm, σ = 1.4 after measuring 50 nanoparticles). Energy-dispersive X-ray spectra (EDX) done on 50 × 50 nm windows were homogeneous over the entire S-layer and confirmed the presence of Cr, Ni, and Cs (Figure 2b).

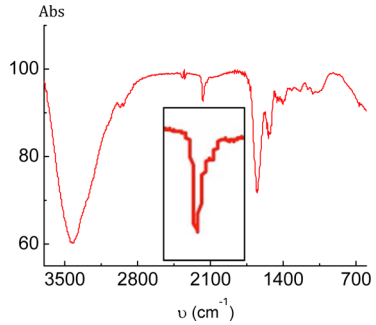

Figure 1. IR powder spectrum of S-layer CrNi, showing the typical bridging cyanide bands (inset).

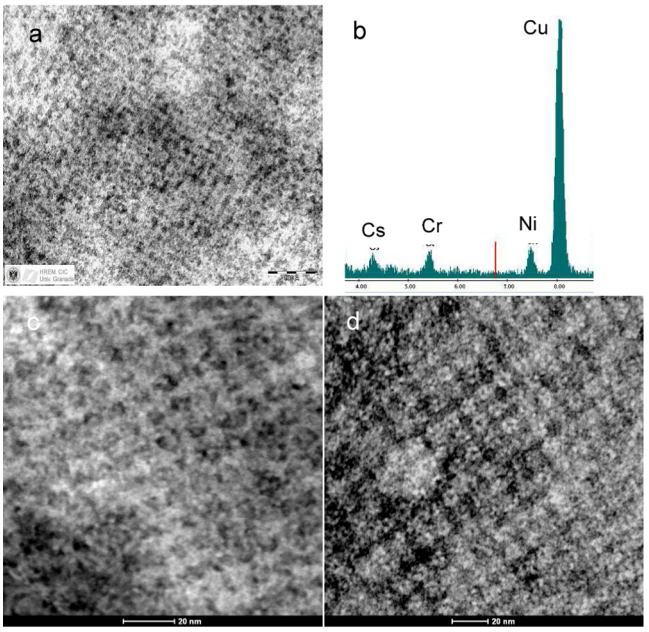

Figure 2. (a) TEM micrograph of the CrNi-S-layer revealing a square (p_4) symmetry pattern of CrNi nanoparticles on the S-layer. It is noticeable that the square lattice structure of the S-layer is visible without the use of contrast, with the electron-dense CrNi nanoparticles themselves providing contrast. (b) EDX spectrum. The Cu peak is due to the sample grid. (c) High-resolution TEM micrograph. (d) HRTEM micrograph of a stained sample.

The TEM image confirms that deposition of CrNi nanoparticles takes place onto the S-layer pores, forming a dense carpet of nanoparticles following a square lattice (p_4) pattern, with a center-to-center spacing of the morphological units of 12 nm, which is typical for the S-layer of *L. sphaericus* (Figure 3). The patterning of CrNi Prussian blue nanoparticles is therefore controlled by the predefined pattern of the S-layer, which serves as a template for their deposition.

All attempts to obtain good AFM images of the S-layer after nanoparticle deposition were unsuccessful. The profile of the S-layer was very irregular, probably due to a heterogeneous filling of its porous network.

Magnetic properties of the deposited nanoparticles were studied using a SQUID magnetometer. The magnetic behavior reveals the expected superparamagnetic behavior, with a blocking temperature (T_B) of around 9 K. Field-cooled (FC) and zero-field-cooled (ZFC) magnetization measurements on the as-prepared CrNi-S-layer sample were carried out within an applied field of 50 G, and a signal of very good quality was

DOI: 10.1021/acs.inorgchem.5b00555
Inorg. Chem. 2015, 54, 6758−6762

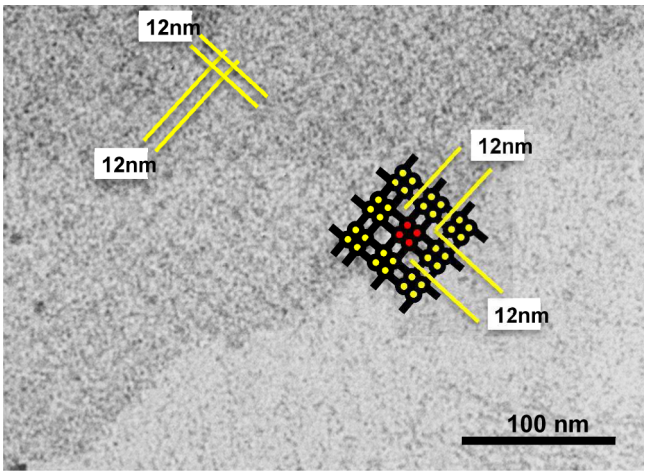

Figure 3. Nanopatterning of CrNi nanoparticles onto the S-layer protein *Lysinibacillus sphaericus* JG-A12. Inserting square p_4 cell units into a TEM micrograph allows visualizing how the pattern of CrNi deposition matches with that of the cubic p_4 S-layer of *L. sphaericus*.

obtained. As can be seen in Figure 4 the two curves diverge below T = 14 K, and the maximum of the ZFC is observed at 9

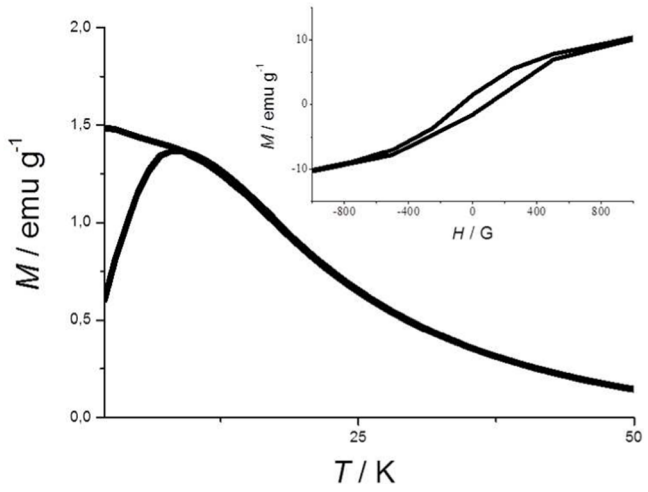

Figure 4. Thermal dependence of the ZFC and FC susceptibility with an applied field of 50 G of a powder CrNi-S-layer. Inset: Hysteresis loop of magnetization at 2 K.

K. This blocking temperature is lower, as expected, than those found for bulk material (Curie temperature of 70 K)[33,34] and for nanoparticles with a higher average size of 9 nm (T_B = 12 K),[9] and it is similar to that observed for the same nanoparticles (average size 6 nm) grafted on a silicon wafer.[6] Otherwise the T_B of the NiCr-S-layer is higher than that of diluted nanoparticles of the same size (T_B = 4 K),[3,35] which might indicate the existence of a dipolar interaction among magnetic NiCr nanoparticles once deposited in the S-layer.

As a consequence of the superparamagnetic behavior of deposited CrNi nanoparticles, a hysteresis loop of magnetization appears below T_B. At temperatures above 9 K no hysteresis is observed. In contrast, a clear hysteresis loop of magnetization is observed at 2 K with a coercive field of 82.5 G (inset Figure 4).

Further evidence of the superparamagnetic behavior of the deposited CrNi nanoparticles is given by the ac susceptibility measurements. Figure 5 displays the temperature dependence of the in-phase (χ') and out-of-phase (χ'') ac susceptibility. The

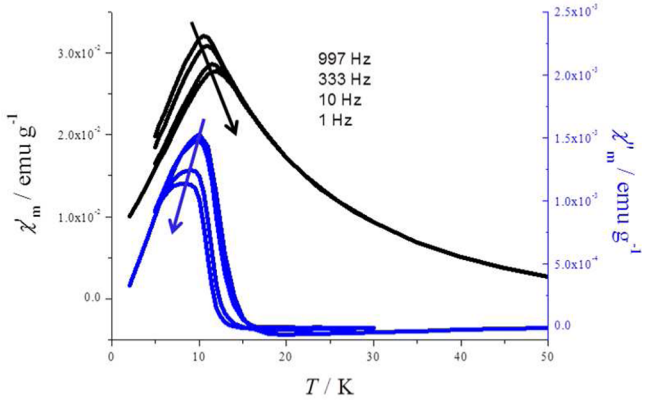

Figure 5. Thermal dependence of the in-phase χ' (black) and out-of-phase χ'' (blue) ac susceptibility of deposited CrNi nanoparticles onto the S-layer at 1, 10, 333, and 997 Hz from left to right.

data of both components exhibit a maximum in the temperature and a shift of this maximum toward higher temperatures at increasing frequencies. For an assembly of isolated single-domain particles the relaxation time of magnetization (τ_0) is expected to follow the Arrhenius law $\tau_0 = \tau_0 \exp(E_a/kT)$. We have found a linear dependence of $\ln(\tau)$ vs $1/T_m$ (T_m = temperature of the maximum of the χ'' peak). From the fitting to the Arrhenius equation, a value of $\tau_0 = 3 \times 10^{-15}$ s was calculated. This value is lower than that expected for isolated magnetic single-domain nanoparticles (10^{-9}–10^{-13} s). In addition to the determination of τ_0, the Mydosh parameter Φ can be calculated, where $\Phi = (T_{max} - T_{min})/T_{max}(\log \nu_{max} - \log \nu_{min})$, with T_{max} and T_{min} being the temperatures of the maxima of the $\chi'' = f(T)$ curves for the two extreme applied frequencies, ν_{max} and ν_{min}, respectively. For noninteracting magnetic single-domain nanoparticles a Φ value higher than 0.1 is expected. For our system a Φ value of 0.07 is obtained, suggesting strongly interacting single-domain nanoparticles or disordered systems (spin glass behavior).[36]

The possible reason that τ_0 is so low is still unclear. In principle, lower values for τ_0 are found for strongly interacting single-domain particles or disordered systems. In this sense, although the existence of interparticle dipolar interactions, despite the dilution of these nanoparticles in the S-layer, cannot be ruled out, an average distance of 12 nm between nanoparticles (Figure 3) seems too large to justify the low value of τ_0. It is more reasonable to consider the existence of some aggregation of nanoparticles at the porous part of the S-layer since more than one nanoparticle of 6 nm could be randomly deposited on a single porous layer of 8 nm. TEM images do not discard this possibility. The existence of some aggregation would explain the low τ_0 value as well as the increase in TB with respect to close magnetic systems.

In summary, we have developed a simple process that is able to fabricate patterns of nanoparticles of a molecule-based magnetic material on a bioplatform, like for the S-layer. These results are encouraging to extend this approach by focusing on molecule-based magnets patterned into domains with controlled shapes and positions on a biosurface, since these domains could be used as magnetic bits as well as in the field of molecular spintronics.

DOI: 10.1021/acs.inorgchem.5b00555
Inorg. Chem. 2015, 54, 6758–6762

EXPERIMENTAL SECTION

Bacterial Growth. *L. sphaericus* JG-A12 cells were grown to late exponential phase in 6 L of nutrient broth medium (8 g/L, Difco), pH 7.0, in 7.5 L bioreactors (Ochs, Bovenden/Lenglern, Germany). All runs were performed in batch culture at 30 °C, at a stirring speed of 500 rpm using a magnetic stirrer and air flow at a rate of 3 L/min. Bacterial growth was monitored by measuring optical densities (OD_{600}) at 600 nm using a Pharmacia Biotech Ultrospec 1000 spectrometer (Amersham Biosciences, Freiburg, Germany). The bacterial cells were harvested by centrifugation at 10000*g* for 20 min.

Preparation of an S-Layer Protein. Intact cells were washed once in a buffer containing 50 mM Tris-HCl, 1 mM $MgCl_2 \cdot 6H_2O$, and 3 mM NaN_3, pH 7.5 (referred to as standard buffer). For removing bacterial flagella, the suspension was homogenized in a rotating-blade IKA T8 blender (IKA Labortechnik, Stauffen, Germany) at maximum speed for 10 min on ice. Flagella-free cells were harvested by centrifugation at 6000*g* for 10 min at 4 °C, resuspended 1:1 in the standard buffer, and mixed with a few crystals of DNase II and RNase. Cells were disintegrated in a 110L microfluidizer (Microfluidics Cooperation, Newton, MA, USA) on ice at a pressure of 960 bar, with three passes. After removing the unbroken cells by centrifugation at 6000*g* for 10 min at 4 °C, cell wall fragments were washed two times in the standard buffer. Plasma membranes were solubilized in 1% Triton X-100 in the standard buffer solution for 10 min at room temperature, and the remaining cell wall fragments were washed twice. Peptidoglycan was hydrolyzed by incubating the samples in a standard buffer solution containing 0.2 mg/mL lysozyme for 6 h at 30 °C. The S-layer fraction was washed several times, resuspended in standard buffer, and stored at 4 °C.

Recrystallization of the S-Layer. For solubilization of the S-layer, protein suspensions each at a concentration of 20 mg/mL were mixed with a volume of 6 M guanidine hydrochloride in 50 mM Tris (pH 7.2) five times as large as that of the protein suspension and stirred at room temperature for 6 h. Nonprotein components were precipitated by centrifugation at 12400*g* for 60 min at 4 °C. The reassembling of the S-layer proteins was performed by dialyzing the supernatant two times against 2 L of 10 mM $CaCl_2$ for 24 h at 4 °C, using dialysis tubes with a molecular weight cutoff of 1000 to 50 000. Reassembled S-layer sheets were harvested by centrifugation at 12400*g* for 60 min at 4 °C, resuspended in 10 mM $CaCl_2$, and stored at 4 °C until use.

Preparation of the NiCr-S-Layer. Following the procedure developed by Malah et al.,[31] nanoparticles of $Cs_xNi[Cr(CN)_6]$ with an average size of 6 nm were obtained in aqueous solution by fast mixing of the precursors in the absence of any organic species. DLS measurements confirmed that no aggregations of particles took place in these conditions. These nanoparticles were then incubated with the S-layer (1 mg/mL) for 24 h at 4 °C. The resulting mixture was purified by centrifugation at 12400*g* for 60 min at 4 °C to isolated the S-layer-containing NiCr nanoparticles. The resulting powder was then dried and isolated. The samples used for TEM were prepared by diluting the powder of theh NiCr-S-layer with Milli-Q water.

Dynamic Light Scattering. To discard some aggregation in the dispersion of $Cs_xNi[Cr(CN)_6]$ before incubation with the S-layer, DLS measurements were done, using a 4700C System from Malvern Instruments. A helium−neon laser operating at 632.8 nm wavelength and about 20 mW was used. The experiments were performed at 25 °C and a scattering angle of 90° (q = 0.018 nm^{-1}). The CONTIN analysis of the intensity autocorrelation function revealed the existence of one population size centered on ∼6 nm.

Electronic Microscopy. A drop of NiCr-S-layer was placed onto a carbon-coated Cu grid (200 mesh). The grid was blotted with filter paper. The same sample was also studied with stain using 1% uranyl acetate. TEM micrographs were taken with a Philips CM-20 and HRTEM with a FEI TITAN G2 microscope. FT-IR analysis was performed on an IR200 spectrometer (ThermoNicolet). Magnetic measurements were performed on lyophilized samples using a magnetometer (Quantum Design MPMS-XL-5) equipped with a SQUID sensor.

AUTHOR INFORMATION

Corresponding Author

*E-mail: josema@ugr.es.

Present Address

⊥Departamento de Microbiología, Universidad de Granada, 18071 Granada, Spain.

Notes

The authors declare no competing financial interest.

ACKNOWLEDGMENTS

This work was funded by MINECO and FEDER (project CTQ2012-32236).

REFERENCES

(1) Dugay, J.; Tan, R. P.; Loubat, A.; Lacroix, L.-M.; Carrey, J.; Fazzini, P. F.; Blon, T.; Mayoral, A.; Chaudret, B.; Respaud, M. *Langmuir* **2014**, *30*, 9028−9035.

(2) Pena, L.; Varon, M.; Konstantinovic, Z.; Balcells, L.; Martinez, B.; Puntes, V. *J. Mater. Chem.* **2011**, *21*, 16973−16977.

(3) Fleury, B.; Volatron, F.; Catala, L.; Brinzei, D.; Rivière, E.; Huc, V.; David, C.; Miserque, F.; Rogez, G.; Baraton, L.; Palacin, S.; Mallah, T. *Inorg. Chem.* **2008**, *47*, 1898−1900.

(4) Ghirri, A.; Candini, A.; Evangelisti, M.; Gazzadi, G. C.; Volatron, F.; Fleury, B.; Catala, L.; David, C.; Mallah, T.; Affronte, M. *Small* **2008**, *4*, 2240−2246.

(5) Clemente-León, M.; Coronado, E.; López-Muñoz, A.; Repetto, D.; Catala, L.; Mallah, T. *Langmuir* **2012**, *28*, 4525−4533.

(6) Coronado, E.; Forment-Aliaga, A.; Pinilla-Cienfuegos, E.; Tatay, S.; Catala, L.; Plaza, J. A. *Adv. Funct. Mater.* **2012**, *22*, 3625−3633.

(7) Cavallini, M.; Gomez-Segura, J.; Ruiz-Molina, D.; Massi, M.; Albonetti, C.; Rovira, C.; Veciana, J.; Biscarini, F. *Angew. Chem., Int. Ed.* **2005**, *44*, 888−892.

(8) Mallah, T.; Thiebaut, S.; Verdaguer, M.; Veillet, P. *Science* **1993**, *262*, 1554.

(9) Entley, W. R.; Girolami, G. S. *Science* **1995**, *268*, 397.

(10) Ferlay, S.; Mallah, T.; Ouahes, R.; Veillet, P.; Verdaguer, M. *Nature* **1995**, *378*, 701.

(11) Sato, O.; Iyoda, T.; Fujishima, A.; Hashimoto, K. *Science* **1996**, *272*, 704.

(12) Sato, Y.; Ohkoshi, S.; Arai, K.; Tozawa, M.; Hashimoto, K. *J. Am. Chem. Soc.* **2003**, *125*, 14590.

(13) Ohkoshi, S.; Tokoro, H.; Hozumi, T.; Zhang, Y.; Hashimoto, K.; Mathoniere, C.; Bord, I.; Rombaut, G.; Verelst, M.; Moulin, C. C. D.; Villain, F. *J. Am. Chem. Soc.* **2006**, *128*, 270.

(14) Coronado, E.; Gimenez-Lopez, M. C.; Levchenko, G.; Romero, F. M.; Garcia-Baonza, V.; Milner, A.; Paz-Pasternak, M. *J. Am. Chem. Soc.* **2005**, *127*, 4580.

(15) Kim, K.; Seo, M.; Means, J.; Meenakshi, V.; Teizer, W.; Zhao, H.; Dunbar, K. R. *Appl. Phys. Lett.* **2004**, *85*, 3872.

(16) Gómez-Segura, J.; Kazakova, O.; Davies, J.; Josephs-Franks, P.; Veciana, J.; Ruiz-Molina, D. *Chem. Commun.* **2005**, 5615.

(17) Martínez, R. V.; García, F.; García, R.; Coronado, E.; Forment-Aliaga, A.; Romero, F. M.; Tatay, S. *Adv. Mater.* **2007**, *19*, 291.

(18) Martinez, R. V.; Martinez, J.; Chiesa, M.; Garcia, R.; Coronado, E.; Pinilla-Cienfuegos, E.; Tatay, S. *Adv. Mater.* **2010**, *22*, 588−591.

(19) Bansal, V.; Bharde, A.; Ramanathan, R.; Bhargava, S. K. *Adv. Colloid Interface Sci.* **2012**, *179*−*182*, 150−168.

(20) Martín, M.; Carmona, F.; Cuesta, R.; Rondón, D.; Gálvez, N.; Dominguez-Vera, J. M. *Adv. Funct. Mater.* **2014**, *24*, 3489−3493.

(21) Carmona, F.; Martin, M.; Galvez, N.; Dominguez-Vera, J. M. *Inorg. Chem.* **2014**, *53*, 8565−8569.

(22) Badelt-Lichtblau, H.; Kainz, B.; Völlenkle, C.; Egelseer, E.-M.; Sleytr, U. B.; Pum, D.; Ilk, N. *Bioconjugate Chem.* **2009**, *20*, 895−903.

(23) Bergkvist, M.; Mark, S. S.; Yang, X.; Angert, E. R.; Batt, C. A. *J. Phys. Chem. B* **2004**, *108*, 8241−8248.

(24) Györvary, E.; Schroedter, A.; Talapin, D. V.; Weller, H.; Pum, D.; Sleytr, U. B. *J. Nanosci. Nanotechnol.* **2004**, *4*, 115−120.

DOI: 10.1021/acs.inorgchem.5b00555
Inorg. Chem. 2015, 54, 6758−6762

(25) Hall, S. R.; Shenton, W.; Engelhardt, H.; Mann, S. *Chem. Phys. Phys. Chem.* **2001**, *3*, 184−186.
(26) Mark, S. S.; Bergkvist, M.; Yang, X.; Teixeira, L. M.; Bhatnagar, P.; Angert, E. R.; Batt, C. A. *Langmuir* **2006**, *22*, 3763−3774.
(27) Mark, S. S.; Bergkvist, M.; Yang, X.; Angert, E. R.; Batt, C. A. *Biomacromolecules* **2006**, *7*, 1884−1897.
(28) Dieluweit, S.; Pum, D.; Sleytr, U. B.; Kautek, W. *Mater. Sci. Eng. C* **2005**, *25*, 727−732.
(29) Merroun, M. L.; Raff, J.; Rossberg, A.; Hennig, C.; Reich, T.; Selenska-Pobell, S. *Appl. Environ. Microbiol.* **2005**, *71*, 5542−5553.
(30) Merroun, M.; Rossberg, A.; Hennig, C.; Scheinost, A. C.; Selenska-Pobell, S. *Mater. Sci. Eng., C* **2007**, *27*, 188−192.
(31) Brinzei, D.; Catala, L.; Louvain, N.; Rogez, G.; Stephan, O.; Gloter, A.; Mallah, T. *J. Mater. Chem.* **2006**, *16*, 2593−2599.
(32) Catala, L.; Brinzei, D.; Prado, Y.; Gloter, A.; Stephan, O.; Rogez, G.; Mallah, T. *Angew. Chem., Int. Ed.* **2009**, *48*, 183−187.
(33) Manuel, E.; Evangelisti, M.; Affronte, M.; Okubo, M.; Train, C.; Verdaguer, M. *Phys. Rev. B* **2006**, *73*, 172406.
(34) Evangelisti, M.; Manuel, E.; Affronte, M.; Okubo, M.; Train, C.; Verdaguer, M. *J. Magn. Magn. Mater.* **2007**, *316*, e569.
(35) Prado, Y.; Lisnard, L.; Heurtaux, D.; Rogez, G.; Gloter, A.; Stéphan, O.; Dia, N.; Rivière, E.; Catala, L.; Mallah, T. *Chem. Commun.* **2011**, *47*, 1051−1053.
(36) Brinzei, D.; Catala, L.; Louvain, N.; Rogez, G.; Stéphan, O.; Gloter, A.; Mallah, T. *J. Mater. Chem.* **2006**, *16*, 2593−2599.

DOI: 10.1021/acs.inorgchem.5b00555
Inorg. Chem. 2015, 54, 6758−6762